4. M. Valden, X. Lai, D. W. Goodman, *Science* **281**, 1647 (1998).
5. U. Heiz, W. D. Schneider, *J. Phys. D Appl. Phys*. **33**, R85 (2000).
6. A. Sanchez *et al.*, *J. Phys. Chem. A* **103**, 9573 (1999).
7. N. Lopez, J. K. Nørskov, *J. Am. Chem. Soc*. **124**, 11262 (2002).
8. H.-G. Boyen *et al.*, *Science* **297**, 1533 (2002).
9. R. Elghanian, J. J. Storhoff, R. C. Mucic, R. L. Letsinger, C. A. Mirkin, *Science* **277**, 1078 (1997).
10. S. Chen *et al.*, *Science* **280**, 2098 (1998).
11. R. L. Whetten *et al.*, *Acc. Chem. Res*. **32**, 397 (1999).
12. A. C. Templeton, W. P. Wuelfing, R. W. Murray, *Acc. Chem. Res*. **33**, 27 (2000).
13. W. D. Luedtke, U. Landman, *J. Phys. Chem*. **100**, 13323 (1996).
14. O. D. Häberlen, S. C. Chung, M. Stener, N. Rösch, *J. Chem. Phys*. **106**, 5189 (1997).
15. I. L. Garzón *et al.*, *Phys. Rev. Lett*. **81**, 1600 (1998).
16. V. Bonacic-Koutecky *et al.*, *J. Chem. Phys*. **117**, 3120 (2002).
17. S. Gilb, P. Weis, F. Furche, R. Ahlrichs, M. M. Kappes, *J. Chem. Phys*. **116**, 4094 (2002).
18. H. Häkkinen, M. Moseler, U. Landman, *Phys. Rev. Lett*. **89**, 033401 (2002).
19. F. Furche *et al.*, *J. Chem. Phys*. **117**, 6982 (2002).
20. L. S. Wang, C. F. Ding, X. B. Wang, S. E. Barlow, *Rev. Sci. Instrum*. **70**, 1957 (1999).
21. L. S. Wang, X. Li, in *Cluster and Nanostructure Interfaces*, P. Jena, S. N. Khanna, B. K. Rao, Eds. (World Scientific, Singapore, 2000), pp. 293–300
22. K. J. Tarlor, C. L. Pettiette-Hall, O. Cheshnovsky, R. E. Smalley, *J. Chem. Phys*. **96**, 3319 (1992).
23. L. S. Wang, H. S. Cheng, J. Fan, *J. Chem. Phys*. **102**, 9480 (1995).
24. X. B. Wang, C. F. Ding, L. S. Wang, *J. Chem. Phys*. **110**, 8217 (1999).
25. O. Gunnarsson *et al.*, *Phys. Rev. Lett*. **74**, 1875 (1995).
26. W. A. de Heer, *Rev. Mod. Phys*. **65**, 611 (1993).
27. P. Pyykkö, N. Runeberg, *Angew. Chem. Int. Ed*. **41**, 2174 (2002).
28. X. Li, B. Kiran, J. Li, H. J. Zhai, L. S. Wang, *Angew. Chem. Int. Ed*. **41**, 4786 (2002).
29. Relativistic density functional calculations on Au_{20} and its anion were performed at the level of a generalized gradient approach using a Perdew-Wang exchange-correlation functional (*30*). The zero-order regular approximation Hamiltonian was used to account for the scalar (mass velocity and Darwin) and spin-orbit relativistic effects (*31*). The standard Slater-type orbital basis sets with quality of triple-zeta plus *p*- and *f* -polarization functions (TZ2P) were used for the valence orbitals of the Au atoms, with frozen core approximation to the [$1s^2$-$4f^{14}$] core. The vertical detachment energies of the anions were calculated via the self-consistent field energy difference between the neutral and anion ground states and the excitation energies of the neutral state calculated by the time-dependent density functional theory method (*32*). All the calculations were accomplished with the Amsterdam Density Functional (ADF 2002) program (*33*). We found that these theoretical methods are suitable for smaller gold clusters, as well as for gold clusters doped with an impurity atom (*28*).
30. J. P. Perdew, Y. Wang, *Phys. Rev. B* **45**, 13244 (1992).
31. E. van Lenthe, E. J. Baerends, J. G. Snijders, *J. Chem. Phys*. **99**, 4597 (1993).
32. S. J. A. van Gisbergen, J. G. Snijders, E. J. Baerends, *Comput. Phys. Commun*. **118**, 119 (1999).
33. ADF 2002, SCM, Theoretical Chemistry, Vrije Universiteit, Amsterdam, Netherlands (www.scm.com).
34. H. Prinzbach *et al.*, *Nature* **407**, 60 (2000).
35. N. T. Wilson, R. L. Johnston, *Eur. Phys. J.* D **12**, 161 (2000).
36. J. Wang, G. Wang, J. Zhao, *Phys. Rev*. B **66**, 354181 (2002).
37. N. Nilius, T. M. Wallis, W. Ho, *Science* **297**, 1853 (2002).
38. The calculations show that the *A*, *B*, and *C* peaks in the PES spectra (Fig. 1) correspond to the triplet and singlet states formed by electron detachment from the HOMO (16e) and HOMO-1 ($29t_2$), wheras the *D* and *E* peaks are due to transitions from HOMO-2 ($18t_1$). See the supporting online material (fig. S1) for the molecular orbital energy-level diagram of T_d Au_{20}.
39. Preliminary calculations on four CO molecules absorbed on the apex and face-center sites reveal a HOMO-LUMO gap of 1.43 and 1.50 eV for the $Au_{20}(CO)_4$ clusters and a binding energy of 0.84 and 0.15 eV per CO molecule, respectively. The large HOMO-LUMO gaps in the naked and CO-adsorbed clusters indicate that the T_d Au_{20} is highly chemically inert and will maintain its structural integrity during catalysis.

40. We thank B. Kiran for helpful discussion. This work was supported by NSF (grant CHE-9817811) and performed at the Environmental Molecular Sciences Laboratory (EMSL), a national scientific user facility sponsored by the U.S. Department of Energy's (DOE's) Office of Biological and Environmental Research and located at Pacific Northwest National Laboratory, operated for DOE by Battelle. All the calculations were performed with supercomputers at the EMSL Molecular Science Computing Facility.

Supporting Online Material

www.sciencemag.org/cgi/content/full/299/5608/864/DC1
Fig. S1
Reference

29 October 2002; accepted 7 January 2003

Carbon Tunneling from a Single Quantum State

Peter S. Zuev,[1] Robert S. Sheridan,[1]* Titus V. Albu,[2] Donald G. Truhlar,[2]* David A. Hrovat,[3] Weston Thatcher Borden[3]*

We observed ring expansion of 1-methylcyclobutylfluorocarbene at 8 kelvin, a reaction that involves carbon tunneling. The measured rate constants were 4.0×10^{-6} per second in nitrogen and 4×10^{-5} per second in argon. Calculations indicated that at this temperature the reaction proceeds from a single quantum state of the reactant so that the computed rate constant has achieved a temperature-independent limit. According to calculations, the tunneling contribution to the rate is 152 orders of magnitude greater than the contribution from passage over the barrier. We discuss environmental effects of the solid-state inert-gas matrix on the reaction rate.

Quantum mechanical tunneling frequently plays an important role in reactions in which a hydrogen atom (*1*), proton (*2*, *3*), or hydride ion (*3*) is transferred. In most organic reactions, motion of carbon is also part of the reaction coordinate, and kinetic isotope effects are consistent with a contribution from carbon motion in some tunneling reactions (*4*). However, evidence for tunneling in reactions that are dominated by carbon motion is rare.

One reaction in which there is good experimental and theoretical evidence for carbon tunneling is the automerization of 1,3-cyclobutadiene (*5*–*7*). In this reaction, the carbons each need to move only about 0.1 Å, resulting in a thin barrier that favors tunneling (*5*). This reaction has been observed at 25 K in an argon matrix (*6*), and tunneling still occurs, despite the solid-state environment of the reactant (*8*).

A few other transformations that involve the making or breaking of C–C σ bonds have been observed at very low temperatures, where there is unlikely to be thermal energy sufficient to allow molecules to surmount any but the most miniscule barriers to reaction (*9*–*11*). The finite rates observed in these reactions suggest that carbon tunneling may be involved. However, the interpretation of these experiments is complicated because in each case, the rate-determining step apparently involves intersystem crossing to an electronic state from which the observed reaction is likely to occur without a barrier.

Tunneling by carbon might play a role in 1,2-shifts in singlet carbenes. The distance between the carbene center and the carbon that migrates to it changes by about 1 Å in these exothermic rearrangements. However, tunneling appears to make only minor contributions to the rates of ring expansions of cyclopropylhalocarbenes in liquid solution at 298 K (*12*). Nevertheless, rearrangements of cyclobutylhalocarbenes to 1-halocyclopentenes are expected to have lower barriers, because in these reactions there is less hyperconjugative stabilization of the reactants and more relief of ring strain in the products than in the ring expansions of cyclopropylhalocarbenes. Indeed, cyclobutylhalocarbenes are shorter-lived in solution at room temperature than are the corresponding cyclopropylhalocarbenes (*13*, *14*).

Here, we report an experimental and com-

[1]Department of Chemistry 216, University of Nevada, Reno, NV 89557, USA. [2]Department of Chemistry and Supercomputer Institute, University of Minnesota, Minneapolis, MN 55455–0431, USA. [3]Department of Chemistry, Box 351700, University of Washington, Seattle, WA 98195–1700, USA.

*To whom correspondence should be addressed. E-mail: rss@unr.edu (R.S.S.); truhlar@umn.edu (D.G.T); borden@chem.washington.edu (W.T.B.)

putational study of carbon tunneling in ring expansion reactions of 1-methylcyclobutylhalocarbenes (**2**) at 8 to 25 K. At such low temperatures, a reactant population can become concentrated in the lowest-energy quantum state, and it should be possible, in principle, to measure the temperature-independent rate constant for reaction from this single vibrational state (*15–20*). Our calculations indicate that the observed ring expansion of **2** does indeed occur at this single–quantum-state limit.

1-Methylcyclobutylhalocarbenes (**2**) were chosen for study because halogen substitution stabilizes the lowest singlet state of carbenes, relative to the triplet; and the methyl group circumvents the 1,2-hydrogen migration that occurs in cyclobutylhalocarbenes, lacking a C-1 substituent (*13*). Chlorodiazirine **1a** (Scheme 1) was synthesized as a precursor of **2a** by a standard Graham reaction (*21–23*).

Photolysis of alkylhalodiazirines generally produces carbenes, which can be characterized at low temperatures. However, when **1a** was irradiated at 334 nm in an N_2 matrix (~1:800) at 8 K, no trace of chlorocarbene **2a** was observed in the infrared (IR) spectrum. The major product was identified as cyclopentene **3a** by comparison of its IR spectrum with that of an authentic sample under the same conditions. A minor amount of the corresponding diazo compound **4a** was also observed. It could be converted into additional **3a** by photolysis with visible light (>500 nm), again, without any **2a** being detected.

Fluorine is a stronger π electron donor than chlorine and thus stabilizes alkyl carbenes more effectively (*13*). Hence, we synthesized fluorodiazirine **1b** from the corresponding bromo compound, using the halodiazirine exchange reaction (*24*). Photolysis at 334 nm of **1b**, matrix-isolated in N_2 at 8 K (~1:800), predominantly produced the corresponding diazo compound **4b**, as evidenced by an intense 2027 cm^{-1} IR absorption. Subsequent irradiation of **4b** with visible light (>550 nm for 30 min) converted the diazo compound partly into fluorocyclopentene **3b**, as shown by comparison of the IR spectrum to that of an authentic sample under the same conditions.

However, another product also formed. It exhibited multiple strong bands in the 1050 to 1150 cm^{-1} region of the IR and a new, weak, visible absorption with a maximum at a wavelength of 430 nm. The subsequent chemistry, as well as comparison of the observed IR and visible absorptions with those computed for **2b** by electronic structure calculations, indicated that the new product was fluorocarbene **2b** (*23*).

Irradiation at 436 nm of a matrix containing **2b** caused the rapid disappearance of the IR bands of the carbene and simultaneous

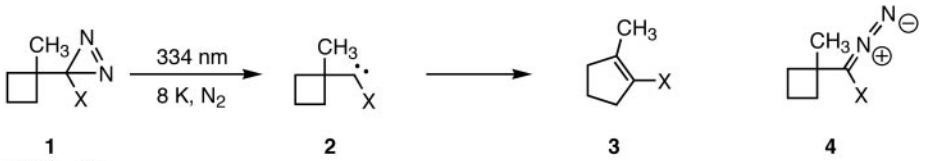

1
(a) X = Cl
(b) X = F

2 **3** **4**

Scheme 1.

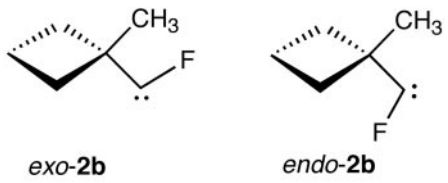

exo-**2b** *endo*-**2b**

Scheme 2.

growth of the IR bands of cyclopentene **3b**. However, even with strict exclusion of light, carbene **2b** also slowly rearranged to cyclopentene **3b** at 8 K.

Electronic structure calculations predict two conformations for **2b**: one with the fluorine exo to the ring and the other with the fluorine endo (Scheme 2). In agreement with the experimental IR spectra, the IR spectra that were calculated for the two conformers were similar and were dominated by strong absorptions in the 1100 cm^{-1} region, attributable to the C–F stretching vibrations.

As expected for the presence of two conformers with dissimilar reactivities, the disappearance of the different IR bands of **2b** showed different temperature and time dependencies. Over a 16-hour period in the dark at 8 K, the 1108 and 1325 cm^{-1} bands of carbene **2b** decayed ~20%, while the bands assigned to cyclopentene **3b** simultaneously grew. However, the IR absorptions attributed to the other conformer of **2b** remained unchanged.

Typically, reactions in low-temperature matrices deviate from first-order kinetics and exhibit rate constants that decrease over time (*10*). This phenomenon, which is generally attributed to distributions of matrix sites with slightly different reaction barriers, usually makes it difficult to extract absolute rate constants. However, decay of the 1108 cm^{-1} IR band during this 16-hour period approximately followed first-order kinetics, giving a rate constant of 4.0×10^{-6} s^{-1} for rearrangement of **2b** at 8 K in N_2.

Both *exo*- and *endo*-**2b** were more labile in Ar than in N_2 matrices. In Ar, both conformers underwent ring expansion at 8 K, and the rate constant for disappearance of the 1108 cm^{-1} band was 4×10^{-5} s^{-1} at 8 K and 9×10^{-5} s^{-1} at 16 K.

When the N_2 matrix was warmed to 16

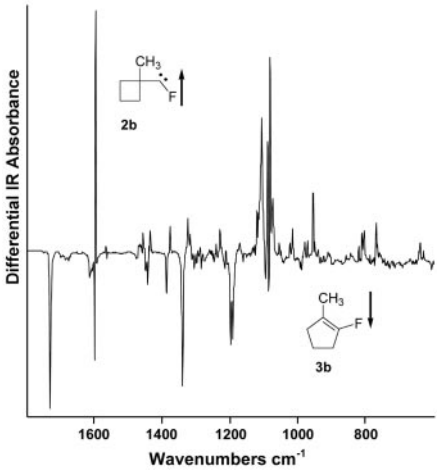

Fig. 1. Difference between IR spectra (generated by >550 nm irradiation of **4b**), taken before and after warming **2b** in an N_2 matrix to 25 K for 2 hours. Absorptions attributed to **2b** are shown as "up bands," and absorptions attributed to **3b** are displayed as "down bands." Bands at 1600 cm^{-1} are absorptions by adventitious H_2O.

K, the 1108 and 1325 cm^{-1} bands disappeared much more rapidly than at 8 K. The absorptions that were attributed to the other conformer of **2b** also began to decay, and the disappearance of these bands was accompanied by a corresponding growth of the IR spectrum of **3b**. At 16 K, plots of the logarithm of the absorbance versus time were slightly nonlinear (*23*), and the rate constants for disappearance of the 1108 cm^{-1} IR band decreased from being initially 12 times larger at 16 K than at 8 K to being only twice as great after 90% reaction. The rate constants for disappearance of the 956 and 1083 cm^{-1} bands, which are attributed to the slower reacting carbene conformer, decreased from an initial value of 6×10^{-6} s^{-1} to 1×10^{-6} s^{-1} after 65% reaction at 16 K. Figure 1 shows the changes that occur in the IR spectrum of **2b** after several hours in an N_2 matrix at 25 K. At this temperature, both carbene isomers rearranged approximately 10 times faster than at 16 K.

Our experimental results are consistent with the faster disappearing set of IR bands belonging to the exo conformer of **2b**, in which the fluorine is appropriately aligned for ring-expansion to **3b**. The slower disap-

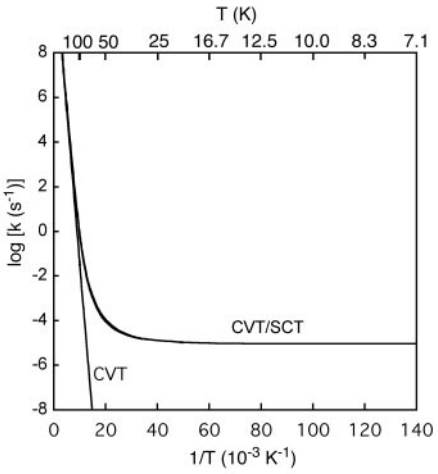

Fig. 2. Arrhenius plot of the logarithm of the rate constant (s^{-1}) for **2b** → **3b**, calculated from CVT theory and with inclusion of tunneling using the SCT approximation.

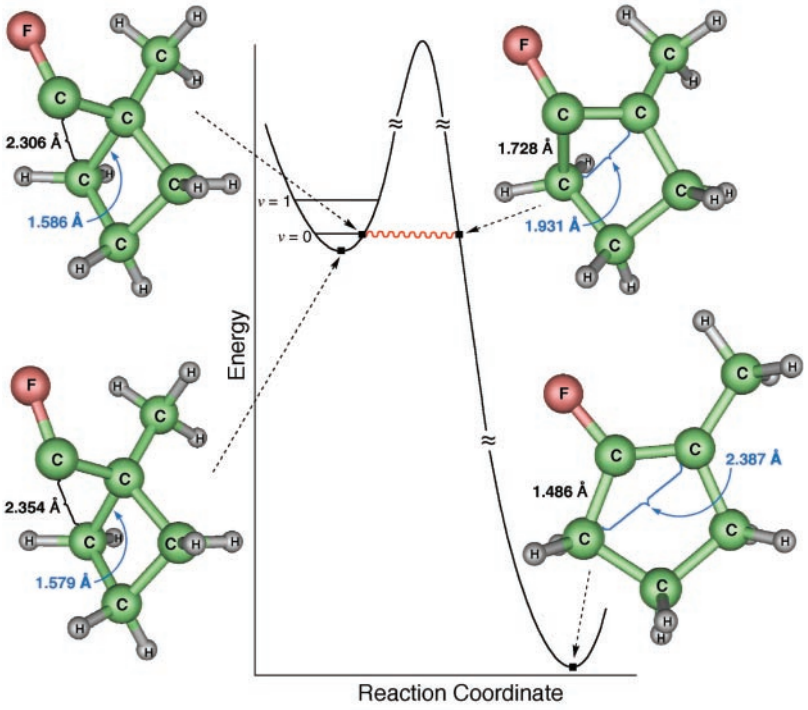

Fig. 3. Four important structures along the reaction path for **2b** → **3b** with $v = 0$. The structures correspond to geometries along the vibrationally adiabatic ground-state potential curve. Two key internuclear distances in each structure are indicated in angstroms.

pearing set of IR bands is assigned to the endo conformer of **2b**, which presumably isomerizes to *exo*-**2b** before undergoing ring expansion to **3b**. The fact that **2b** can be observed, whereas **2a** cannot be, is attributable to the greater stabilizing effect of fluorine than of chlorine on carbenes (*13*).

We found that the rate of rearrangement of **2b** in Ar is just a factor of 2 greater at 16 K than at 8 K and that tripling the absolute temperature accelerates the ring-expansion of **2b** in N_2 only by a factor of about 100. These findings are inconsistent with a thermally activated process. Instead, our observations indicate that ring expansion of this carbene occurs by carbon-atom tunneling.

To confirm that carbon-atom tunneling provides a viable explanation of our experiments, we calculated the expected tunneling rates in the ring expansions of **2a** to **3a** and **2b** to **3b**, using the same computational methodology that we employed in studying 1,2-shifts in other carbenes (*12*). The rate constants were calculated by direct dynamics; that is, the potential energy surface and its first and second derivatives with respect to nuclear positions were obtained directly from electronic structure calculations, as they were needed for the dynamics computations (*25*). Modified Perdew-Wang hybrid density functional theory, with one parameter optimized for kinetics (*26*), was used in conjunction with the 6–31+$G(d,p)$ basis set (*27*) for the electronic structure calculations. The dynamics were treated by canonical variational transition state (CVT) theory (*28*), and tunneling contributions were included by using the small-curvature tunneling (SCT) approximation (*29*). The calculations neglected the effects of the solid-state matrix environment on the reaction.

Rearrangement of chlorocarbene **2a** to chlorocyclopentene **3a** was computed to have a zero-point inclusive energy of reaction of $\Delta E_0 = -358$ kJ mol^{-1}, with a zero-point inclusive barrier height of $\Delta E^{\ddagger} = 13$ kJ mol^{-1}. The corresponding ring expansion of fluorocarbene **2b** was calculated to be less exoergic ($\Delta E_0 = -328$ kJ mol^{-1}) and to have a barrier ($\Delta E^{\ddagger} = 27$ kJ mol^{-1}) that is twice as large as the barrier for the rearrangement of **2a**. Both barriers are far too high to be surmounted by thermal activation at 8 to 25 K.

Arrhenius plots of the calculated rate constants for the rearrangement of **2b** to **3b** (Fig. 2) show that the low-temperature limit of 9.1×10^{-6} s^{-1} (corresponding to a half-life of 21 hours) is achieved within 10% for temperatures (T) < 20 K. In agreement with the hypothesis that the rearrangement of **2a** to **3a** is too fast to allow detection of **2a** under our experimental conditions, we calculate a much larger limiting rate constant of 1.4×10^{4} s^{-1} (corresponding to a half-life of 10^{-4} s) for rearrangement of **2a**. In this case also, the limiting low-temperature rate constant is achieved within 10% for $T < 20$ K.

The calculations confirm that the rearrangement of **2** to **3** at 8 K is dominated by tunneling. When tunneling is not included, the rate constants at 8 K are calculated to be smaller by a factor of 2×10^{52} for **2a** and 2×10^{152} for **2b**. Furthermore, unlike the case at the temperatures at which most tunneling reactions have been observed, at 8 K the ring expansion of **2b** occurs almost exclusively from the $v = 0$ vibrational ground state (i.e., without any appreciable thermal activation). The reaction coordinate mode was calculated to have a frequency of 69 cm^{-1}; tunneling from the $v = 1$ excited vibrational state of this mode contributes only 4×10^{-2}% of the rate at 8 K.

Figure 3 shows four important structures along the reaction path, specifically, the reactant (**2b**), the geometries at the beginning and ending termini of the tunneling path from the $v = 0$ vibrational level, and the product (**3b**). The changes in three-dimensional positions of the individual atoms at the termini of the tunneling path can be used to calculate the distances moved by each of the atoms during the tunneling event, and these distances provide a more detailed picture than the changes in bond lengths that are shown in Fig. 3. The longest distance traveled by any of the carbon atoms during the tunneling event is 0.44 Å for the methylene group that makes a new bond to the carbenic carbon in the product. The other carbons move 0.11 to 0.33 Å, the fluorine moves 0.23 Å, and the hydrogens move 0.09 to 0.56 Å.

The tunneling reaction changes character as the temperature increases. At 16 K, the fraction of reaction occurring out of the $v = 1$ vibrational level increases to 6%, and at 39 K the contributions to the reaction from the $v = 0$ and $v = 1$ levels become equal. The transition at this temperature from dominant ground-state tunneling to dominant thermally activated tunneling is associated with the maximum curvature of the calculated Arrhenius plot for **2b** in Fig. 2.

This change in the tunneling mechanism is especially evident in the change in the Arrhenius activation energy, defined by $E_a = -Rd\ln k/d(1/T)$, where R is the gas constant and k is the rate constant. E_a increases from a negligible 0.3 J mol^{-1} at 8 K to 0.45, 1.2, and 23.6 kJ mol^{-1} at 30, 40, and 150 K, respectively. The vanishing of the activation energy at low temperatures (i.e., in the region of near-zero slope in Fig. 2) is a dramatic consequence of tunneling from only the $v = 0$ vibrational level.

At 216 K, the nontunneling ("over-barrier") component of the rate becomes equal to the tunneling ("through-barrier") contribution, and at 298 K the over-barrier component is 2.7 times larger than the through-barrier contribution. Above room temperature, E_a increases only slowly, from 25.5 kJ mol^{-1} at 298 K to 26.0 kJ mol^{-1} at 400 K. Thus, in this temperature range, the experimental Arrhenius plot for the rearrangement of **2b** to **3b** should appear to be quite linear, because the small degree of curvature, caused by the temperature dependence of E_a, would probably not be detectable. Tunneling still contributes to the rate, but like passage over the barrier, tunneling is a thermally activated process in this temperature regime.

The calculated rate constants at 8 K for rearrangement of **2a** (1.4×10^4 s^{-1}) and **2b** (9.1×10^{-6} s^{-1}) are consistent with both the failure to detect chlorocarbene **2a** and the observation of rearrangement of fluorocarbene **2b** with a half-life on the order of tens of hours at this temperature. Because theory predicts that raising the temperature from 8 to 16 K will produce a negligible change in rate, the observed increases in the rate constant for the rearrangement of **2b** to **3b** are interpreted as environmental effects on the carbene lifetime. In particular, ring expansion may be inhibited by the rigidity of the matrix, so that matrix softening could be responsible for this temperature dependence. Matrix softening would also explain the need to increase the temperature to 16 K, in order for the less reactive conformer *endo*-**2b** to rearrange in N_2, presumably by first isomerizing, by tunneling, to the more reactive conformer *exo*-**2b** (*30*). The greater reactivity of both conformers in Ar than in N_2 and the smaller temperature dependence of the rate of rearrangement in Ar are consistent with the expectation that Ar should be the softer matrix.

The dominance of tunneling in the rearrangement of **2** to **3** at low temperatures suggests that heavy-atom tunneling may be more facile than is generally recognized. In addition, the direct observation of the rearrangement of **2b** to **3b** at the low-temperature limit for this reaction suggests new possibilities for understanding, controlling, and tuning chemical reactivity at the single–quantum-state level of resolution.

References and Notes

1. B. C. Garrett *et al*., *J. Am. Chem. Soc.* **108**, 3515 (1986).
2. D. G. Truhlar *et al*., *Acc. Chem. Res.* **35**, 341 (2002).
3. A. Kohen, J. P. Klinman, *Chem. Biol.* **6**, R191 (1999).
4. D. J. Miller, R. Subramanian, W. H. Saunders Jr., *J. Am. Chem. Soc.* **103**, 3519 (1981).
5. B. K. Carpenter, *J. Am. Chem. Soc.* **105**, 1700 (1983).
6. A. M. Orendt *et al*., *J. Am. Chem. Soc.* **110**, 2648 (1988).
7. R. Lefebvre, N. Moiseyev, *J. Am. Chem. Soc.* **112**, 5052 (1990).
8. B. R. Arnold, J. G. Radziszewski, A. Campion, S. S. Perry, J. Michl, *J. Am. Chem. Soc.* **113**, 692 (1991).
9. S. L. Buchwalter, G. L. Closs, *J. Am. Chem. Soc.* **101**, 4688 (1979).
10. M. B. Sponsler, R. Jain, F. D. Coms, D. A. Dougherty, *J. Am. Chem. Soc.* **111**, 2240 (1989).
11. W. Sander, G. Bucher, F. Reichel, D. Cremer, *J. Am. Chem. Soc.* **113**, 5311 (1991).
12. T. V. Albu *et al.*, *J. Phys. Chem. A* **106**, 5323 (2002).
13. R. A. Moss, G. J. Ho, W. Liu, *J. Am. Chem. Soc.* **114**, 959 (1992).
14. G. J. Ho *et al*., *J. Am. Chem. Soc.* **111**, 6875 (1989).
15. V. I. Goldanskii, M. D. Frank-Kamenetskii, I. M. Barkalov, *Science* **182**, 1344 (1973).
16. K. Toriyama, K. Numone, M. Iwaski, *J. Am. Chem. Soc.* **99**, 5823 (1977).
17. D. P. Kiryukhin, I. M. Barkalov, V. I. Goldanskii, *J. Chem. Phys.* **76**, 1013 (1979).
18. G. C. Hancock, C. A. Mead, D. G. Truhlar, A. J. C. Varandas, *J. Chem. Phys.* **91**, 3492 (1989).
19. S. E. Wonchoba, W.-P. Hu, D. G. Truhlar, *Phys. Rev. B* **51**, 9985 (1995).
20. N. Balakrishnan, A. Dalgarno, *Chem. Phys. Lett.* **341**, 652 (2001).
21 W. J. Graham, *J. Am. Chem. Soc.* **87**, 4396 (1965).
22. P. Rempala, R. S. Sheridan, *J. Chem. Soc. Perkin Trans.* **2**, *2257* (1999).
23. Materials and methods are available as supporting material on *Science* Online.
24. R. A. Moss *et al*., *J. Am. Chem. Soc.* **107**, 2743 (1985).
25. D. G. Truhlar, M. S. Gordon, *Science* **249**, 491 (1990).
26. B. J. Lynch, P. L. Fast, M. Harris, D. G. Truhlar, *J. Phys. Chem. A* **104**, 4811 (2000).
27. W. J. Hehre, L. Radom, P. v. R. Schleyer, J. A. Pople, *Ab Initio Molecular Orbital Theory* (Wiley, New York, 1986).
28. D. G. Truhlar, B. C. Garrett, *Annu. Rev. Phys. Chem.* **35**, 159 (1984).
29. Y.-P. Liu *et al*., *J. Am. Chem. Soc.* **115**, 2408 (1993).
30. The CVT/SCT rate constant for this isomerization reaction at 8 to 16 K is computed to be 2.6×10^{-4} s^{-1} and is essentially the rate constant for tunneling. This value is about a factor of 10 larger than the rate of disappearance of the less reactive conformer at 8 K, even in an Ar matrix. However, the calculated rate constant is only a factor of 4 larger than the rate constant for disappearance of this isomer at 16 K in an N_2 matrix, where some matrix softening presumably occurs.

31. We thank NSF for support of this research at the Universities of Nevada (Reno), Minnesota, and Washington. P.S.Z. and R.S.S. also acknowledge the Donors of the American Chemical Society Petroleum Research Fund for partial support of this research.

Supporting Online Material

www.sciencemag.org/cgi/content/full/299/5608/867/DC1
Materials and Methods
Figs. S1 and S2
References

10 October 2002; accepted 27 December 2002

Atomic-Resolution Imaging of Oxygen in Perovskite Ceramics

C. L. Jia, M. Lentzen, K. Urban*

Using an imaging mode based on the adjustment of a negative value of the spherical-aberration coefficient of the objective lens of a transmission electron microscope, we successfully imaged all types of atomic columns in the dielectric $SrTiO_3$ and the superconductor $YBa_2Cu_3O_7$. In particular, we were able to view the oxygen atoms which, due to their low scattering power, were not previously accessible, and this allowed us to detect local nonstoichiometries or the degree of oxygen-vacancy ordering. This technique offers interesting opportunities for research into oxides, minerals, and ceramics. In particular, this holds for the huge group of perovskite-derived electroceramic materials in which the local oxygen content sensitively controls the electronic properties.

Thin films of Ba- and Sr-based perovskites have great potential for application, in particular as high-permittivity dielectrics in microelectronics or nonvolatile memory devices. Research on the structure and properties of these materials has shown that variations in chemical composition in the bulk or in connection with lattice defects are detrimental to materials properties and device performance (*1*, *2*). Above all, it is the local oxygen content which reacts sensitively to cation disorder or lattice strain. The same applies to the cuprate high-temperature superconductors. In their perovskite-derived structure, the oxygen occupancy of certain lattice sites sensitively controls the charge carrier density in the superconducting planes (*3*, *4*).

The microstructure of perovskites can be studied by means of high-resolution transmission electron microscopy (HRTEM). Under suitable conditions it is possible to image the cation columns projected along the viewing direction. Because the cations have a high nuclear charge, their scattering power is high, resulting in strong phase contrast. In comparison, due to the relatively low scattering power, it is difficult to image the oxygen sublat-

Institute of Solid State Research, Research Center Juelich, D-52425 Juelich, Germany.

*To whom correspondence should be addressed. E-mail: k.urban@fz-juelich.de